scientific reports

OPEN

Alkali metal doping of black phosphorus monolayer for ultrasensitive capture and detection of nitrogen dioxide

Azam Marjani[1,2], Mehdi Ghambarian[3] & Mohammad Ghashghaee[4]✉

Black phosphorus nanostructures have recently sparked substantial research interest for the rational development of novel chemosensors and nanodevices. For the first time, the influence of alkali metal doping of black phosphorus monolayer (BP) on its capabilities for nitrogen dioxide (NO_2) capture and monitoring is discussed. Four different nanostructures including BP, Li-BP, Na-BP, and K-BP were evaluated; it was found that the adsorption configuration on Li-BP was different from others such that the NO_2 molecule preferred a vertical stabilization rather than a parallel configuration with respect to the surface. The efficiency for the detection increased in the sequence of Na-BP < BP < K-BP < Li-BP, with the most significant improvement of + 95.2% in the case of Li doping. The Na-BP demonstrated the most compelling capacity (54 times higher than BP) for NO_2 capture and catalysis (− 24.36 kcal/mol at HSE06/TZVP). Furthermore, the K-doped device was appropriate for both nitrogen dioxide adsorption and sensing while also providing the highest work function sensitivity (55.4%), which was much higher than that of BP (10.4%).

In recent decades, chemosensors and biosensors have been studied intensely due to the increasing importance of safety precautions and environmental protections. Sensors have been used in many industries for the detection of harmful compounds. Nitrogen dioxide (NO_2) with a biting odor is considered as one of the most vital noxious gases in terms of air pollution. Also, it is used for the commercial production of nitric acid. Hence, modern society has a strong motivation to explore more sensitive NO_2 detectors for controlling its impact on the environment and protection of human health and safety[1]. Various types of sensors are actively studied for this purpose. Some well-established classes of detectors including solid electrolytes, electrochemical sensors, graphene-based systems, as well as metal oxides have been introduced[2].

Novel nanostructured and two-dimensional (2D) materials are actively pursued toward different optical and sensing applications[3–11]. Investigations of black phosphorus structures have been carried out by many researchers after its successful fabrication for different optical, biomedical, and environmental applications[12–17]. These 2D nanomaterials have outstanding heat as well as electron conductivities due to their great anisotropic properties[18–21]. Moreover, black phosphorus possess appropriate chemical and fire resistance[22,23].

With regard to NO_2, efficient detectors have been introduced, which have been reviewed elsewhere[1]. The research on such sensors is of great interest in different research groups exploring the properties of 2D materials[18,24–27]. Black phosphorus itself has provided physisorption capabilities for several gases, such as NO_2[18,28]. However, BP has been recorded to outperform molybdenum disulfide (MoS_2) for the nitrogen dioxide analysis in terms of the sensitivity threshold and quick regeneration[29]. An increased conductance sensitivity down to 5 ppb of nitrogen dioxide has been recorded for the multilayer BP detector[30]. In another study of nitrogen dioxide adsorption capabilities, Si embedding into graphene was quite effectual[31]. another study has shown that graphene/NiO heterostructures were helpful for NO_2 sensing[32]. Similarly, the NiO-decorated BP slab has shown (116 times) stronger adsorption relative to the pristine layer for nitrogen dioxide capture and catalysis[18]. Aluminum decoration of BP has also shown useful for the capture of this toxic molecule with the adsorption energy of 3.96 eV[33]. Recently, the SnO monolayer slab has been presented to be auspicious for nitrogen dioxide

[1]Department for Management of Science and Technology Development, Ton Duc Thang University, Ho Chi Minh City, Viet Nam. [2]Faculty of Applied Sciences, Ton Duc Thang University, Ho Chi Minh City, Viet Nam. [3]Gas Conversion Department, Faculty of Petrochemicals, Iran Polymer and Petrochemical Institute, P.O. Box 14975-112, Tehran, Iran. [4]Department of Petrochemical Synthesis, Faculty of Petrochemicals, Iran Polymer and Petrochemical Institute, P.O. Box 14975-112, Tehran, Iran. ✉email: m.ghashghaee@ippi.ac.ir
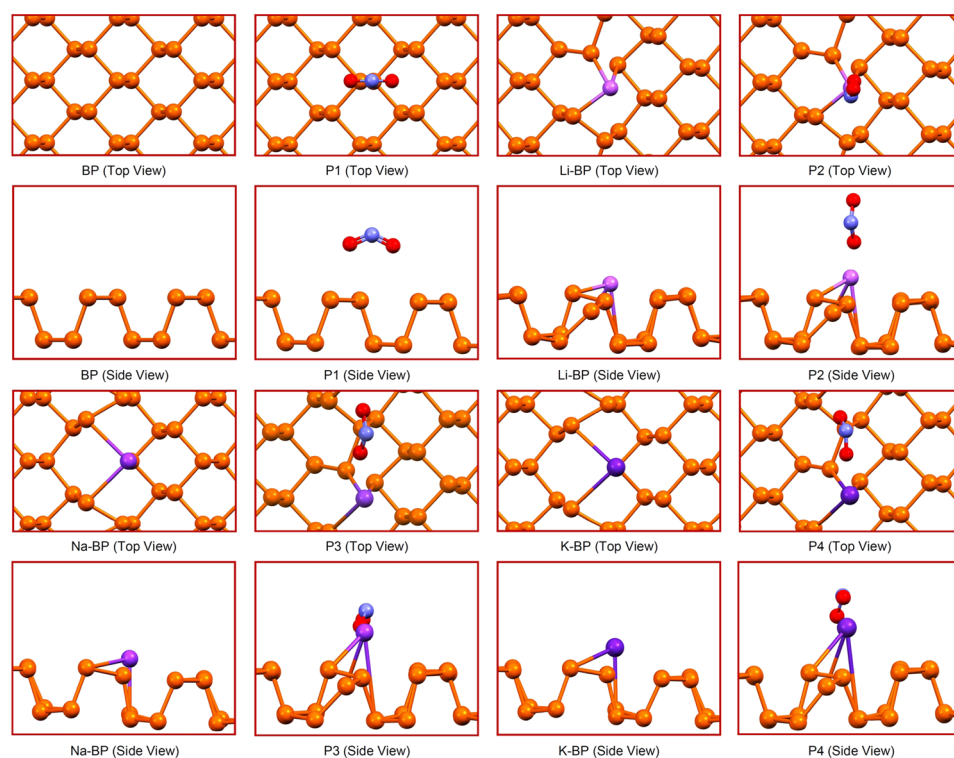
Figure 1. Relaxed configurations of the intact and working chemosensors obtained at the PBE/SVP computational level. The color indicators include orange for the P atoms, red for the O atoms, blue for the N atoms, and purple for the alkali metal (Li, Na, K) atoms. The images were drawn using Mercury 3.6.

capture and monitoring[34]. Among 2D nanomaterials, gallium nitride demonstrated significant bandgap alterations of 1.65 eV after the exposure to nitrogen dioxide[35]. Recently, the effectiveness of defect and ZnO species incorporation into the BP monolayer was shown for the NO_2 monitoring and removal, respectively[19].

Doping is a useful tool for the modulation of the anisotropic characteristics of the 2D materials for the sensing applications. For instance, Zhou et al. have found that the embedding of transition metals, particularly Ti and Au, can significantly enhance the chemical reactivity of graphene, thus leading to activation of the NO_2 molecule for the graphene-based catalysis applications[36]. One may reasonably postulate that the effective doping of black phosphorus can enhance its capabilities toward the adsorption of NO_2 molecule. In spite of the intriguing characteristics of black phosphorus, still little is known about the possible effects of such modifications on either the adsorption strength or sensitivity. In the same line, we explored the effects of alkali metal (Li, Na, and K) doping of BP monolayer on the sensitivity to the NO_2 molecule. The nitrogen dioxide detection using black phosphorene has not been studied conclusively. The current research study deals with investigation of different BP structures in terms of the electronic as well as energetic properties for nitrogen dioxide adsorption.

As will be shown in the following, the suggested modifications can make substantial improvements in both the adsorption and sensing of NO_2 on black phosphorene depending on the alkali metal employed. In a broader sense, the reported data would help supply a deeper understanding for the rational development of novel phosphorene-based nanomaterials for the adsorption and sensing of gaseous pollutants.

Results and discussion

Several BP-based sensors have been inspected here, which include the pristine (BP) and alkali-doped M-BP nanomaterials (M = Li, Na, K). The methodology for the construction of the sensors is given in the Supplementary Information. Several modifiers, including transition metal (TM) elements, have been examined in the phosphorene functionalization and doping, as reviewed elsewhere[13]. Here, we have chosen the lightest members of the alkali metals, being among the ten most abundant elements in Earth crust[37]. As such, the modifications at hand would be less expensive and environmentally benign.

The sensors with optimized geometries at the rest and operating conditions are shown in Fig. 1. From Fig. 1, we observe that the nitrogen dioxide molecule interacted through its two O atoms with the P atoms of the unmodified pristine layer while stabilizing in the armchair orientation with the O–N–O plane (P1). The stabilization of the NO_2 molecule on the M-doped sensors was different. Notably, the related structure with Li-BP was the most different such that the molecule preferred a vertical arrangement with respect to the surface while interacting through an O atom (P2). This observation is in correspondence with the absence of the 3d orbitals in lithium and the lower protrusion of the Li atom compared to the other dopants (vide infra). The NO_2 molecule on both Na-BP and K-BP was optimized more similarly to P1 except that the O–N–O angle was stabilized in

Sensor	d	E_{form}	ΔE_{ads}
BP	2.79	–	− 0.45
Li-BP	1.82	− 1.63	− 9.68
Na-BP	0.31	− 1.17	− 24.36
K-BP	0.50	− 1.27	− 20.59

Table 1. Adsorption distances (d, Å), formation energies (E_{form}, eV), and the corresponding sorption energies (ΔE_{ads}, kcal/mol) of the NO$_2$ molecule on the original and modified sensors at the HSE06/TZVP level of theory.

Structure	r(M–P)	r(N–O)	ε	τ	μ	η	ω
BP	–	–	–	–	5.00	0.73	17.18
P1	–	1.21	40.5	19.3 fs	5.07	0.60	21.57
Li-BP	2.81 ± 0.45	–	–	–	4.53	0.83	12.37
P2	3.01 ± 0.57	1.23 ± 0.03	79.1	14.8 ns	5.47	0.53	28.07
Na-BP	3.08 ± 0.17	–	–	–	4.43	0.71	13.88
P3	3.58 ± 0.70	1.25	22.4	33.2 s	5.28	0.78	17.89
K-BP	3.37 ± 0.06	–	–	–	3.97	0.64	12.32
P4	3.82 ± 0.62	1.24 ± 0.01	43.5	132.1 ms	5.29	0.64	21.71

Table 2. Various specifications of the investigated sensors at the HSE06/TZVP level: the mean M–P bond length [r(M–P), Å], the mean N–O bond length [r(N–O), Å], the efficiency of the analysis (ε, %), the regeneration time of the sensor (τ, fs–s), the chemical potential factor (μ, eV), the global hardness of the structure (η, eV), and the electrophilicity indicator (ω, eV). The efficiency was defined using Eq. (7). Also, the visible light radiation at 343 K was considered for the calculation of the recovery time.

the zigzag direction, with one of the oxygen atoms tending to approach the dopant center (P3 and P4). In both cases, the adsorption of NO$_2$ molecule also led to the more projection of the metal atom away from the surface (vide infra); but, the solid matrix integrity was not lost in either case owing to the small distortions.

The formation energy values for the M-BP materials were calculated as follows:[21,38]

$$E_{form} = (E_{M-BP} + \mu_P) - (E_{BP} + \mu_M). \tag{1}$$

Here, E_{BP} and E_{M-BP} denote the total energies of the unmodified and alkali-doped BP slabs.; the symbol μ_P denotes the chemical potential of phosphorus. The pure phosphorene chemical potential was considered in this study. The symbol μ_M refers to the chemical potential of the M dopant. The energetics of the nitrogen dioxide molecule on various phosphorene-based structures was determined as follows:[21,39–41]

$$\Delta E_{ads} = E_{op} - (E_{gas} + E_{sensor}) \tag{2}$$

in which the subscript op refers to the adsorption configuration (the operating device), and gas denotes the nitrogen dioxide molecule.

The energetic data have been supplied in Table 1. The formation energy for the incorporation of alkali metal was predicted to be negative in all cases indicating that the incorporation of these metal elements into the structure would be highly favorable, and high doping concentrations are plausible thermodynamically. The sequence of Na-BP < K-BP < Li-BP was found for the energetic favorability of the modification. In spite of the fact that the adsorption of nitrogen dioxide on the pristine layer was weak, the gaseous molecule was almost tightly chemisorbed on the alkali-modified sensor, and the adsorption strength was sequenced as BP < Li-BP < K-BP < Na-BP (up to − 24.36 kcal/mol at HSE06/TZVP). The equilibrium distance for the NO$_2$ molecule varied in the range of 0.31–2.79 Å, inversely correlating with the adsorption strength (Table 1). It was concluded that the NO$_2$ adsorption strength had been increased 54 times upon sodium doping. Such enhancement implies that the alkali-doping is a useful means of increasing the capability of black phosphorene for NO$_2$ capture.

One can see from the geometrical data that the average distance for the M–P bonds increased in the order of Li-BP < Na-BP < K-BP (Table 2). Furthermore, the adsorption of NO$_2$ led to an elongation of the r(M–P) values by 7.1%, 16.2%, and 13.4%, correlating with the adsorption strength. In the same line, the r(N–O) values increased slightly from 1.20 Å for the free molecule to 1.21, 1.23, 1.25, and 1.24 Å in P1, P2, P3, and P4, respectively. The geometrical features demonstrate that the stronger the adsorption, the shorter the adsorption distance, and the longer the M–P and N–O bonds at the adsorption site.

The induced magnetic moment in the operating mode was found to be 1.0 μ_B due to the stabilization of the nitrogen dioxide molecule on the surface. The spin moment (μ_s) contribution from nitrogen dioxide was sequenced as P3 (0.03 μ_B) < P4 (0.27 μ_B) < P2 (0.63 μ_B) < P1 (0.93 μ_B). The charge gaps of the non-magnetic structures were determined as follows:
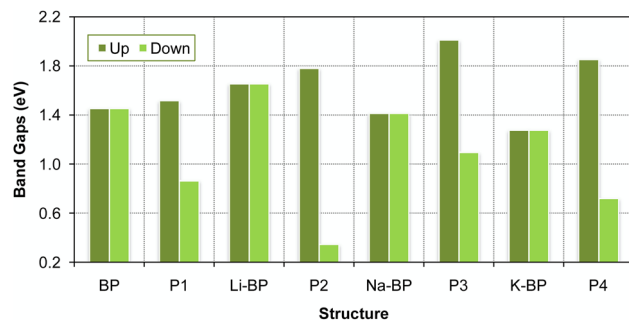
Figure 2. Electronic bandgaps of the unmodified and alkali-modified sensors at the off state and working conditions for nitrogen dioxide detection at the HSE06/TZVP computational level.

$$E_g = E_{LUCO} - E_{HOCO}, \tag{3}$$

where E_{LUCO} refers to the lowest unoccupied crystal orbital (LUCO) energy level with the unit of eV. Also, E_{HOCO} denotes the highest occupied crystal orbital (HOCO) energy level (eV). Similarly, the spin-conserving gaps for both up and down spin channels could be determined using the following equations:[15]

$$E_{g\uparrow} = E_{LUCO\uparrow} - E_{SOCO\uparrow} \tag{4}$$

and

$$E_{g\downarrow} = E_{LUCO\downarrow} - E_{SOCO\downarrow} \tag{5}$$

in which E_{SOCO} denotes the single occupied crystal orbital (SOCO) energy level (eV). The nanosensor signal is determined by the alteration in the electrical conductance defined as follows:[15,42,43]

$$\sigma = AT^{3/2} \exp\left(\frac{-E_g}{2k_B T}\right) \tag{6}$$

in which T signifies the working temperature (K), k_B signifies the Boltzmann constant (eV K^{-1}), and A represents the constant of proportionality (in electrons m^{-3} K$^{-3/2}$). The sensors bandgaps at the off state as well as during operation are provided in Fig. 2. As evinced by these charts, all sensors kept their semiconducting nature through modification and operation, and no half-metallic behavior was induced. The bandgap of the pristine layer was obtained as 1.46 eV, which indicates that there is a great agreement between the obtained value and the experimental range (1.0–1.5 eV) for the single-layer BP nanodevice[44]. This observation confirms the suitability of the method applied here[15,38].

The original bandgap (BP) was slightly expanded after lithium doping, but it was slightly shrunk after sodium and potassium doping (Fig. 2). However, it should be pointed out that the amount of bandgap in the up-spin channel was enlarged with the NO$_2$ sensitivity, while it was decreased in the down-spin gap after the interaction of the analyte for all sensors. A huge variation in the bandgap was observed in the case of Li doping compared to the other cases, which implied the higher sensitivity of this sensor to the NO$_2$ molecule. The electronic band structures of the sensors are presented in Fig. 3. The determined band structure for the pristine phosphorene was fully consistent with the Brillouin zone (BZ) data reported in the literature[45], indicating the existence of a direct bandgap at the Γ point of the BZ[15]. A similar type of (direct) bandgap was obtained in the case of Li-BP and Na-BP. Nonetheless, the electronic band structure for the K-BP nanodevice exhibited an indirect X → Y nature. In terms of band alignment, the energy levels of the conduction band minimum (CBM) and the valence band maximum (VBM) both shifted upward upon alkali doping with the magnitude of the changes following the sequence of Li-BP < Na-BP < K-BP. The relative energy position of the Fermi level is discussed under the work function (vide infra). When the type of semiconduction was concerned, almost all metal impurities were neutral, thus retaining the intrinsic behavior of the original BP material intact. However, the analyte behaved as an acceptor and led to a p-type semiconductor in all operating cases.

The detector quality or efficiency was evaluated from the relative alterations of the bandgap:[18]

$$\varepsilon = 100\left(\frac{|E_g - E_0|}{E_g}\right) \tag{7}$$

in which ε represents the detector efficiency, while the initial state of the sensor was indicated by 0 and the symbol E_g is the bandgap at the operating conditions[18]. Based on this definition, the amount of E_g is negative when there is a shortening bandgap due to the interactions with the nitrogen dioxide. Table 2 reports the central operating data for the unmodified and alkali-doped sensors for the NO$_2$ molecule analysis[19]. The absolute efficiency changed in the order of Na-BP < BP < K-BP < Li-BP, indicating the efficiency changes relative to the unmodified BP of + 95.2, − 44.6, and + 7.4% with the Li, Na, and K doping, respectively. Therefore, the Li-doped sensor has registered the highest efficiency (79.1%) for NO$_2$ detection. So, it could be concluded that the pristine phosphorene became
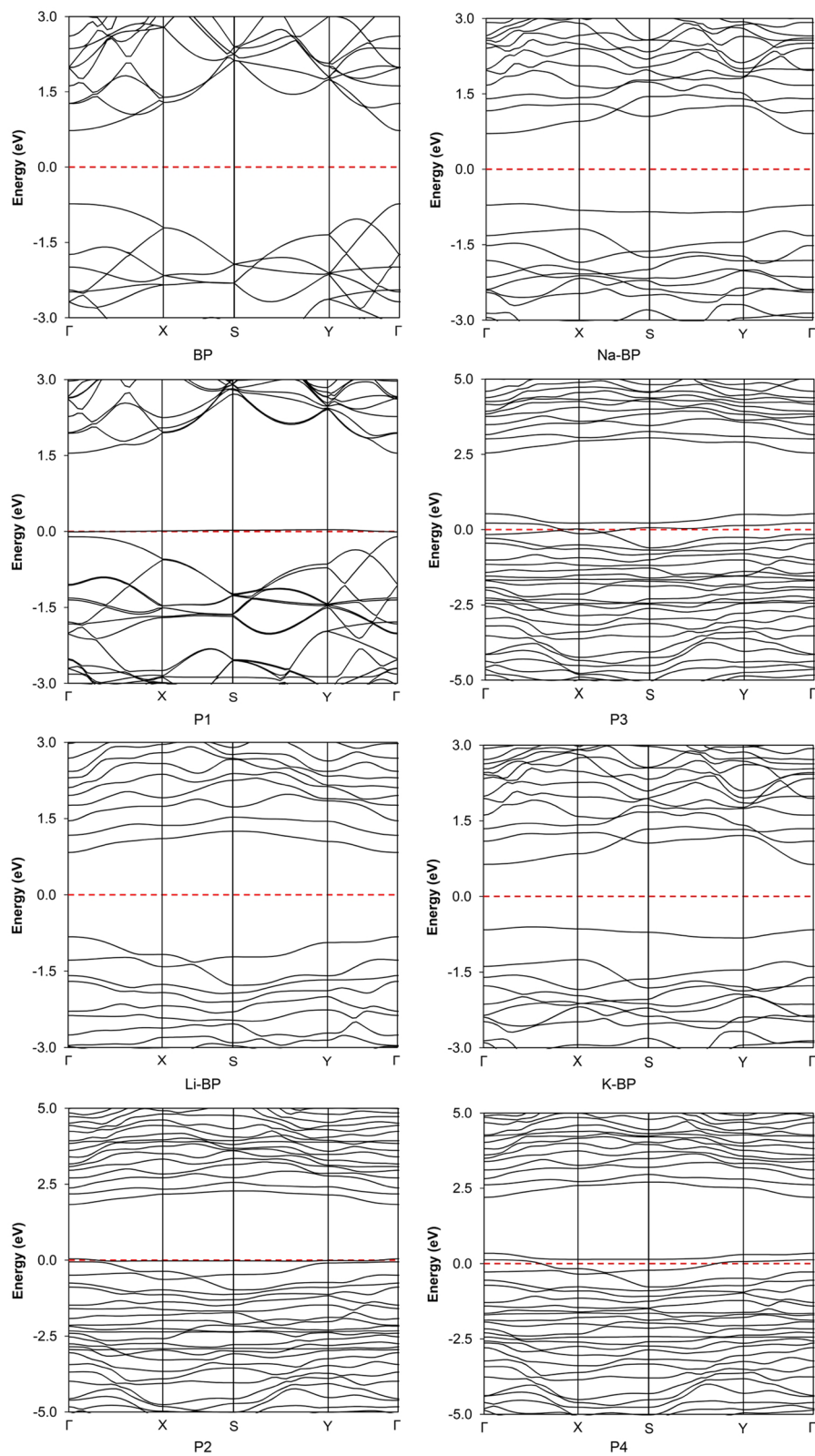
Figure 3. Band structures of the unmodified and alkali-modified sensors at the off and operating states at the HSE06/TZVP computational level. The outputs have been obtained from Burai 1.3.

more capable of NO$_2$ monitoring and removal with the incorporation of K and Li in its structure. On the basis of the intermediate adsorption energy (− 9.68 kcal/mol) released on Li-BP, it would be an ideal choice for NO$_2$ detection (vide infra).

The sensors reusability is one of the most critical parameters in order to appraise its performance. Conventional transition state theory (TST) was applied to the calculation of the recovery time using the amount of adsorption energy:[43,46]

$$\tau = \nu_0^{-1} \exp\left(\frac{-\Delta E_{\mathrm{ads}}}{k_{\mathrm{B}} T}\right) \qquad (8)$$

in which ΔE_{ads} shows the adsorption energy (kcal/mol) determined from Eq. (2), and ν_0 refers to the attempt frequency (s^{-1})[18]. The calculated data provided in Table 2 delineate the speed of regeneration. Although BP provided the lowest recovery time (19.3 fs), it should be mentioned that the obtained recovery period was extremely short for stable monitoring. Furthermore, the alkali-doped sensors were capable of being regenerated under visible radiation at 343 K. Interestingly, the most sensitive sensor (Li-BP) had a recovery time of 14.8 ns at these conditions. Even the calculated recovery time in the slowest case (33.2 s for Na-BP) was quite reasonable compared to the performance of novel tellurene and borophene materials[47,48]. Therefore, the findings point to the conclusion that the alkali doping can adjust the electronic properties of the phosphorene layer to be a sensitive and reusable sensor for nitrogen dioxide detection and monitoring. In addition, the Na-doped material would be more appropriate for NO$_2$ removal and catalysis owing to the relatively high retention time and the stronger adsorption. Moreover, the K-BP material would be considered as an ultrasensitive sensor with reasonable reusability at mild conditions.

Table 2 shows more indicators for the evaluation of the sensors in terms of reactivity of the structures. The indicators were selected based on Koopman's theorem[43,49,50]. The chemical potential is the first indicator, and can be expressed as follows:[15]

$$\mu = -\chi, \qquad (9)$$

$$\chi = (I + A)/2 \approx -(E_{\mathrm{HOCO}} + E_{\mathrm{LUCO}})/2 \qquad (10)$$

in which I represents the ionization potential, χ is the electronegativity, and A signifies the electron affinity. Another expression can be given for the magnetic complexes:[18,51,52]

$$\chi = -[(E_{\mathrm{SOCO}\uparrow} + E_{\mathrm{LUCO}\uparrow}) + (E_{\mathrm{SOCO}\downarrow} + E_{\mathrm{LUCO}\downarrow})]/4. \qquad (11)$$

Also, the following equations were used for the estimation of the global hardness (Eq. 12), the spin potential at zero net spin transfer (Eq. 13), and the electrophilicity (Eq. 14):[18]

$$\eta = (E_{\mathrm{LUCO}} - E_{\mathrm{HOCO}})/2, \qquad (12)$$

$$\eta = [(E_{\mathrm{LUCO}\uparrow} + E_{\mathrm{LUCO}\downarrow}) - (E_{\mathrm{SOCO}\uparrow} + E_{\mathrm{SOCO}\downarrow})]/4, \qquad (13)$$

$$\omega = \mu^2/(2\eta). \qquad (14)$$

Table 2 contains such indicators for the four sensors at the HSE06/TZVP computational level[15]. The data showed that the chemical potential and electrophilicity values increased with the adsorption of the NO$_2$ molecule. As indicated, the sensor efficiency correlated well with the electrophilicity of the operating sensor.

Another consideration is that the adsorption of nitrogen dioxide may alter the work function of the chemiresistive nanodevice. In such cases, the material would be a work function detector. Equation (15) was used for the evaluation of the changes in the work function during the detection process:[19]

$$\varphi = E_{\mathrm{vac}} - E_{\mathrm{F}}, \qquad (15)$$

where E_{F} denotes the Fermi energy level, and E_{vac} is the vacuum energy (the electrostatic potential in the vacuum)[15]. The obtained magnitudes are shown in Fig. 4. The base-case work function was 5.14 eV at the HSE06/TZVP level of theory, which was in excellent agreement with the theoretical magnitude of 5.03 eV[53] and the experimental measurement of 5.30 eV[54] for a single-layer phosphorene. The work function of the sensor itself was decreased in the order of K-BP < Na-BP < Li-BP < BP. Moreover, the adsorption of NO$_2$ resulted in an enhancement in the work function of all sensors. These changes were sequenced as BP (10.4%) < Li-BP (30.5%) < Na-BP (35.6%) < K-BP (55.4%), indicating that the K-BP sensor would be an excellent work function sensor (5.3 times better than the pristine BP at the HSE06/TZVP) for the NO$_2$ detection. Meanwhile, we note that the Na-BP has shown quite high work function sensitivity to NO$_2$ while requiring higher temperatures for a fast recovery. Higher sensitivity and obvious reusability for nitrogen dioxide detection were obtained with the Li-doped phosphorene sensor.

The frontier molecular orbital (FMO) dispersions of the adsorption adducts are illustrated in Fig. 5. The alkali doping changed the orbital distribution, while the density localization did not occur precisely at the dopant center. Specifically, the HOCO densities of the Li-BP and K-BP sensors were changed substantially. The nitrogen dioxide molecule was involved mostly in the LUCO of P1; however, a negligible contribution in HOCO could be found for the analyte. Over the alkali-modified sensors, the NO$_2$ molecule showed the lowest contribution to the FMO with the Li-BP surface (P2). In terms of Na-BP performance (P3), the amount of HOCO electron density located on the analyte was more significant, which also exhibited an apparent LUCO involvement by this
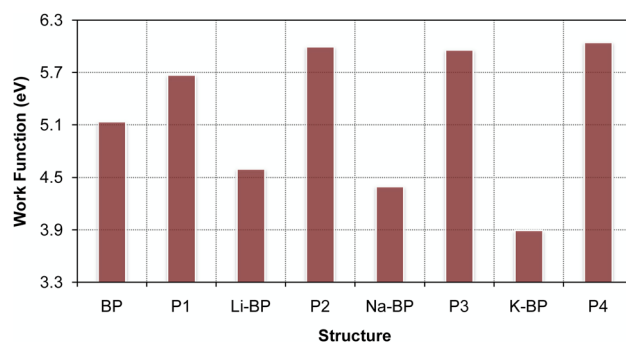
Figure 4. Work function sensitivity chart of the phosphorene-based materials for nitrogen dioxide capture and monitoring at the HSE06/TZVP computational level.
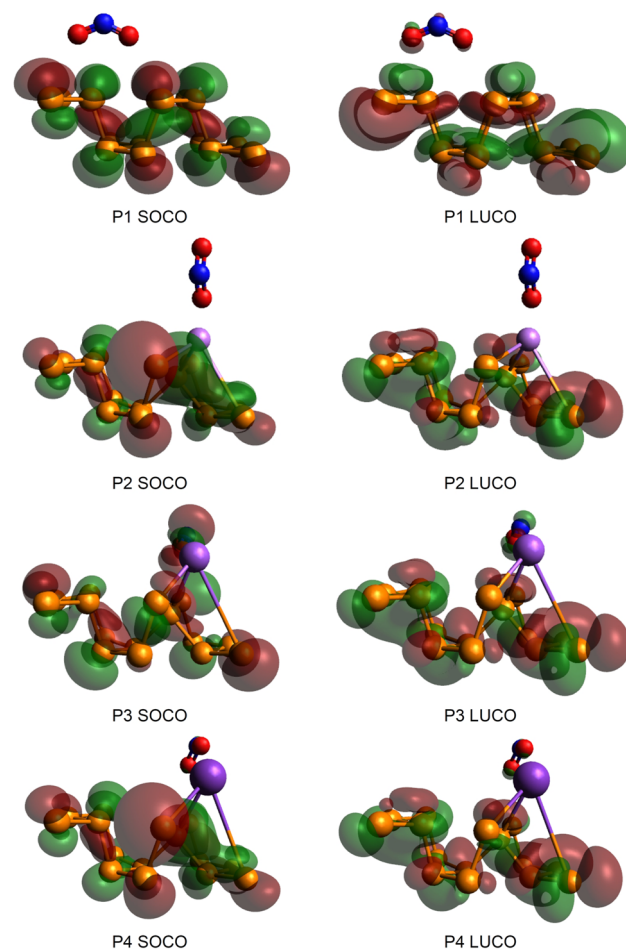
Figure 5. HOCO/LUCO dispersions of the working chemosensors at the HSE06/TZVP computational level. The orbitals have been drawn in Avogadro 1.2.0.

fragment. Finally, the nitrogen dioxide adsorption on K-BP directed to a weak delocalization of LUCO toward this fragment with almost no density localization in the case of HOCO. These observations qualitatively confirm the sequence of adsorption energies explained above.

The alkali-doped phosphorene structures can be discussed in terms of the projected (PDOS) and total (TDOS) density of states, as shown in Fig. 6 for the four sensors after the exposure to nitrogen dioxide. Also shown in Fig. 6 are the overlap population (OPDOS) curves of the NO_2 molecule at the surface. As one can see in these plots, the partial density plots of the NO_2 molecule were almost the same in the P1 and P2 configurations, due mainly to the relatively small involvement of the (NO_2) analyte in the FMO distributions (vide supra). In the P3 and P4 structures, however, the corresponding PDOS pattern upshifted by ca. 1.3 eV, thus leading to a more
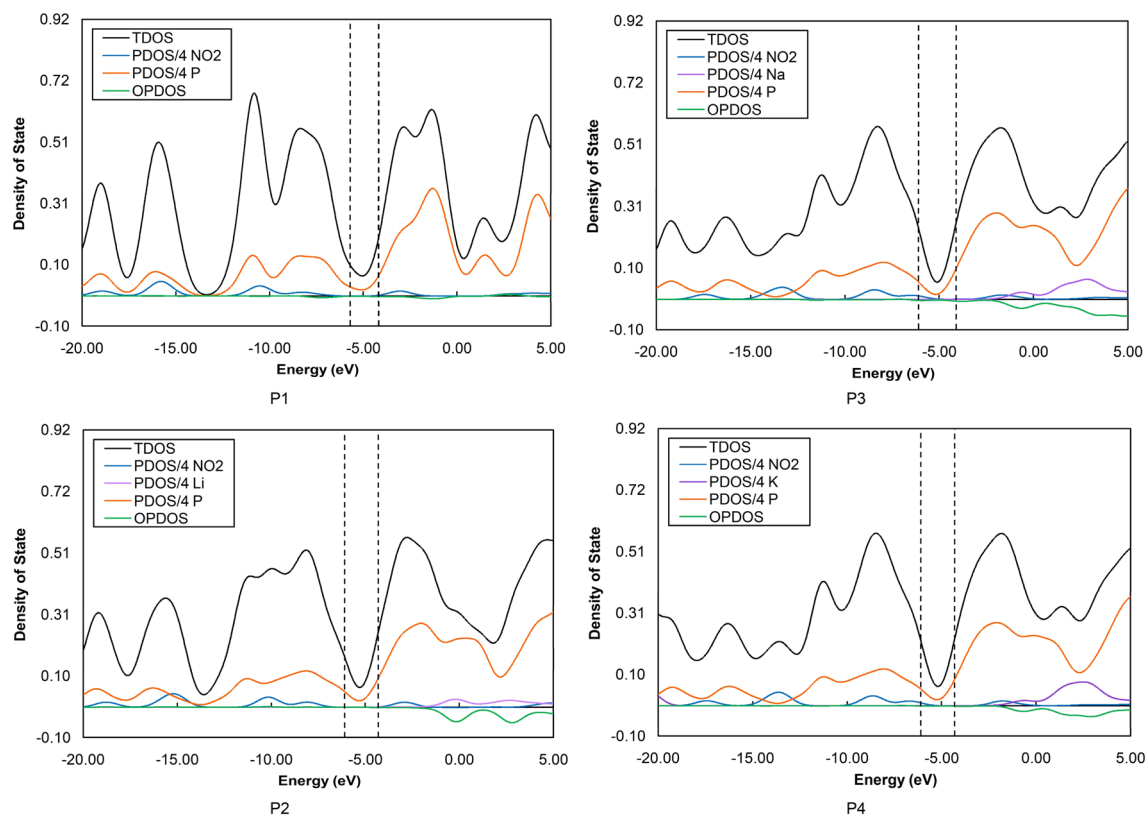
Figure 6. Projected (PDOS) and total (TDOS) profiles of the density of states for nitrogen dioxide monitoring with the four BP-based chemiresistive nanomaterials at the HSE06/TZVP computational level. The spectra have been obtained from Multiwfn 3.3.8.

pronounced contribution to the lower edge of the bandgap. This observation further supports our discussion of the FMO distributions. Further in the same line, the OPDOS curve in P2 indicated the non-bonding nature over an almost wide energy range around the Fermi level. Moving to P3, however, we observed anti-bonding behavior near the Fermi level. The orbitals of nitrogen dioxide molecule and phosphorus atoms were slightly hybridized at − 8.0 eV in the bonding regions of P2. Similar behavior was observed at − 8.2 and − 19.0 eV in the case of P1. Such observation was not the case for the rest of the sensors. Overall, these explanations describe how the most sensitive sensors behave differently for NO_2 detection.

Conclusion

In summary, this article studied for the first time the comparative influence of alkali metal doping of the pristine BP layer on its performance in terms of elimination and detection of nitrogen dioxide with the aid of periodic quantum-chemical calculations. While nitrogen dioxide was stabilized in a horizontal configuration aligned in the black phosphorene armchair direction and the zigzag directions of Na-BP and K-BP, the lowest-energy configuration on Li-BP was different such that the molecule preferred a vertical arrangement with an oxygen atom pointing to the surface. The formation energies indicated the feasibility of alkali doping at high concentrations following the order of Na-BP < K-BP < Li-BP. However, the Na-BP displayed the strongest analyte chemisorption (− 24.36 kcal/mol at HSE06/TZVP). Significant correlations were found between the adsorption distance and the M–P and N–O bond length alterations with the adsorption strength. For all nanosensors investigated here, the bandgap changed oppositely depending on the spin channel. While the type of bandgap was retained after Li and Na doping, an indirect X → Y transfer preference was observed in the K-BP band structure. The Li-doped phosphorene material showed the highest sensitivity (79.1%) toward the NO_2 molecule (increased by 95.2% compared to the pristine BP). Interestingly, the most sensitive material in this series (Li-BP) had an optimal recovery time of 14.8 ns at 343 K. Meanwhile, the Na-BP material was found to be more appropriate for nitrogen dioxide capture and catalysis. On the grounds of the global indicators, a connection could be established between the responsivity and the electrophilicity at the working conditions. While BP was the least effective for NO_2 removal, the K-doped material was applicable for nitrogen dioxide removal and detection, while also turning out to provide the highest work function sensitivity (55.4%) for the NO_2 detection. In summary, we may conclude that the Li-doped monolayer can be considered as an ultrasensitive and recoverable NO_2 chemosensor. Furthermore, the potassium embedding in the BP pristine layer can transform it into a dual-purpose device for both nitrogen dioxide removal/catalysis and sensing.

Methods

Periodic DFT computations were conducted[19] in the environments of CP2K[55], NWChem 6.5[56], Multiwfn 3.3.8[57], and Burai 1.3 software[58]. The pictorial outputs were obtained with Mercury 3.6[59] and Avogadro 1.2.0.[60] Further details of the computational approach are given in the Supplementary Information.

References

1. Wang, T. *et al.* A review on graphene-based gas/vapor sensors with unique properties and potential applications. *Nano-Micro Lett.* **8**, 95–119. https://doi.org/10.1007/s40820-015-0073-1 (2016).
2. Hunter, G. W. *et al.* Editors' choice—critical review—a critical review of solid state gas sensors. *J. Electrochem. Soc.* **167**, 037570. https://doi.org/10.1149/1945-7111/ab729c (2020).
3. Qiu, M. *et al.* Theoretical study on the rational design of cyano-substituted P3HT materials for OSCs: Substitution effect on the improvement of photovoltaic performance. *J. Phys. Chem. C* **119**, 8501–8511. https://doi.org/10.1021/acs.jpcc.5b01071 (2015).
4. Huang, H. *et al.* Donor–acceptor conjugated polymers based on thieno[3,2-b]indole (TI) and 2,1,3-benzothiadiazole (BT) for high efficiency polymer solar cells. *J. Mater. Chem. C* **4**, 5448–5460. https://doi.org/10.1039/c6tc00929h (2016).
5. Qiu, M. *et al.* Strategy to manipulate molecular orientation and charge mobility in D-A type conjugated polymer through rational fluorination for improvements of photovoltaic performances. *J. Phys. Chem. C* **120**, 22757–22765. https://doi.org/10.1021/acs.jpcc.6b03756 (2016).
6. Qiu, M. *et al.* Toward an understanding of how the optical property of water-soluble cationic polythiophene derivative is altered by the addition of salts: The Hofmeister effect. *J. Phys. Chem. C* **117**, 21870–21878. https://doi.org/10.1021/jp407430y (2013).
7. Qiu, M. *et al.* WO₃ with surface oxygen vacancies as an anode buffer layer for high performance polymer solar cells. *J. Mater. Chem. A* **4**, 894–900. https://doi.org/10.1039/c5ta08898d (2016).
8. Marjani, A., Ghashghaee, M., Ghambarian, M. & Ghadiri, M. Scandium doping of black phosphorene for enhanced sensitivity to hydrogen sulfide: Periodic DFT calculations. *J. Phys. Chem. Solids* **148**, 109765. https://doi.org/10.1016/j.jpcs.2020.109765 (2020).
9. Ghashghaee, M. & Shirvani, S. Catalytic transformation of ethylene to propylene and butene over an acidic Ca-incorporated composite nanocatalyst. *Appl. Catal. A Gen.* **569**, 20–27. https://doi.org/10.1016/j.apcata.2018.10.017 (2019).
10. Ghashghaee, M., Azizi, Z. & Ghambarian, M. Conductivity tuning of charged triazine and heptazine graphitic carbon nitride (g-C₃N₄) quantum dots via nonmetal (B, O, S, P) doping: DFT calculations. *J. Phys. Chem. Solids* **141**, 109422. https://doi.org/10.1016/j.jpcs.2020.109422 (2020).
11. Ghashghaee, M., Azizi, Z. & Ghambarian, M. Quantum-chemical calculations on graphitic carbon nitride (g-C3N4) single-layer nanostructures: Polymeric slab vs. quantum dot. *Struct. Chem.* **31**, 1137–1148. https://doi.org/10.1007/s11224-020-01496-x (2020).
12. Castellanos-Gomez, A. *et al.* Isolation and characterization of few-layer black phosphorus. *2D Mater.* **1**, 025001. https://doi.org/10.1088/2053-1583/1/2/025001 (2014).
13. Ghambarian, M., Azizi, Z. & Ghashghaee, M. Functionalization and doping of black phosphorus. In *Black Phosphorus: Synthesis, Properties and Applications*, 1–30 (Springer, New York, 2020) https://doi.org/10.1007/978-3-030-29555-4_1.
14. Ghashghaee, M., Azizi, Z. & Ghambarian, M. Substitutional doping of black phosphorene with boron, nitrogen, and arsenic for sulfur trioxide detection: A theoretical perspective. *J. Sulfur Chem.* **41**, 399–420. https://doi.org/10.1080/17415993.2020.1752692 (2020).
15. Ghambarian, M., Azizi, Z. & Ghashghaee, M. Remarkable improvement in phosgene detection with a defect-engineered phosphorene sensor: First-principles calculations. *Phys. Chem. Chem. Phys.* **22**, 9677–9684. https://doi.org/10.1039/d0cp00427h (2020).
16. An, D. *et al.* Progress in the therapeutic applications of polymer-decorated black phosphorus and black phosphorus analog nanomaterials in biomedicine. *J. Mater. Chem. B* **8**, 7076–7120. https://doi.org/10.1039/d0tb00824a (2020).
17. Xie, Z. *et al.* Emerging combination strategies with phototherapy in cancer nanomedicine. *Chem. Soc. Rev.* https://doi.org/10.1039/d0cs00215a (2020).
18. Ghadiri, M., Ghashghaee, M. & Ghambarian, M. Influence of NiO decoration on adsorption capabilities of black phosphorus monolayer toward nitrogen dioxide: Periodic DFT calculations. *Mol. Simul.* **46**, 1062–1072. https://doi.org/10.1080/08927022.2020.1802023 (2020).
19. Ghashghaee, M. & Ghambarian, M. Defect engineering and zinc oxide doping of black phosphorene for nitrogen dioxide capture and detection: Quantum-chemical calculations. *Appl. Surf. Sci.* **523**, 146527. https://doi.org/10.1016/j.apsusc.2020.146527 (2020).
20. Ghadiri, M., Ghashghaee, M. & Ghambarian, M. Defective phosphorene for highly efficient formaldehyde detection: Periodic density functional calculations. *Phys. Lett. A* **384**, 126792. https://doi.org/10.1016/j.physleta.2020.126792 (2020).
21. Ghadiri, M., Ghashghaee, M. & Ghambarian, M. Mn-Doped black phosphorene for ultrasensitive hydrogen sulfide detection: Periodic DFT calculations. *Phys. Chem. Chem. Phys.* **22**, 15549–15558. https://doi.org/10.1039/d0cp02013c (2020).
22. Eswaraiah, V., Zeng, Q., Long, Y. & Liu, Z. Black phosphorus nanosheets: Synthesis, characterization and applications. *Small* **12**, 3480–3502. https://doi.org/10.1002/smll.201600032 (2016).
23. Ghashghaee, M., Ghambarian, M. & Azizi, Z. Chemistry of black phosphorus. In *Black Phosphorus: Synthesis, Properties and Applications*, 59–72 (Springer, New York, 2020) https://doi.org/10.1007/978-3-030-29555-4_3.
24. Ghashghaee, M., Ghambarian, M. & Azizi, Z. Theoretical insights into sensing of hexavalent chromium on buckled and planar polymeric carbon nitride nanosheets of heptazine and triazine structures. *Mol. Simul.* **46**, 54–61. https://doi.org/10.1080/08927022.2019.1674447 (2019).
25. Ghambarian, M., Ghashghaee, M., Azizi, Z. & Balar, M. Molecular interactions of MeOH and EtOH with black phosphorus monolayer: A periodic density functional study. *Phys. Chem. Res.* **7**, 435–447. https://doi.org/10.22036/pcr.2019.172026.1594 (2019).
26. Khandelwal, A., Mani, K., Karigerasi, M. H. & Lahiri, I. Phosphorene – The two-dimensional black phosphorous: Properties, synthesis and applications. *Mater. Sci. Eng. B* **221**, 17–34. https://doi.org/10.1016/j.mseb.2017.03.011 (2017).
27. Ghashghaee, M., Azizi, Z. & Ghambarian, M. Adsorption of iron(II, III) cations on pristine heptazine and triazine polymeric carbon nitride quantum dots of buckled and planar structures: Theoretical insights. *Adsorption* **26**, 429–442. https://doi.org/10.1007/s10450-019-00197-0 (2020).
28. Kou, L., Frauenheim, T. & Chen, C. Phosphorene as a Superior Gas Sensor: Selective Adsorption and Distinct I-V Response. *J. Phys. Chem. Lett.* **5**, 2675–2681. https://doi.org/10.1021/jz501188k (2014).
29. Cho, S.-Y. *et al.* Superior chemical sensing performance of black phosphorus: Comparison with MoS₂ and graphene. *Adv. Mater.* **28**, 7020–7028. https://doi.org/10.1002/adma.201601167 (2016).
30. Abbas, A. N. *et al.* Black phosphorus gas sensors. *ACS Nano* **9**, 5618–5624. https://doi.org/10.1021/acsnano.5b01961 (2015).
31. Chen, Y., Gao, B., Zhao, J.-X., Cai, Q.-H. & Fu, H.-G. Si-doped graphene: An ideal sensor for NO- or NO₂-detection and metal-free catalyst for N₂O-reduction. *J. Mol. Model.* **18**, 2043–2054. https://doi.org/10.1007/s00894-011-1226-x (2012).

32. Hoa, L. T., Tien, H. N., Luan, V. H., Chung, J. S. & Hur, S. H. Fabrication of a novel 2D-graphene/2D-NiO nanosheet-based hybrid nanostructure and its use in highly sensitive NO_2 sensors. *Sens. Actuat. B Chem.* **185**, 701–705. https://doi.org/10.1016/j.snb.2013.05.050 (2013).

33. Kuang, A. *et al.* Acidic gases (CO_2, NO_2 and SO_2) capture and dissociation on metal decorated phosphorene. *Appl. Surf. Sci.* **410**, 505–512. https://doi.org/10.1016/j.apsusc.2017.03.135 (2017).

34. Yao, Y. *et al.* Density functional theory insight towards high sensitivity for NO, NO_2 and O_2 over monolayer SnO. *Mater. Res. Express* **6**, 095078. https://doi.org/10.1088/2053-1591/ab3016 (2019).

35. Yong, Y. *et al.* Two-dimensional tetragonal GaN as potential molecule sensors for NO and NO_2 detection: A first-principle study. *ACS Omega* **2**, 8888–8895. https://doi.org/10.1021/acsomega.7b01586 (2017).

36. Zhou, M., Lu, Y.-H., Cai, Y.-Q., Zhang, C. & Feng, Y.-P. Adsorption of gas molecules on transition metal embedded graphene: A search for high-performance graphene-based catalysts and gas sensors. *Nanotechnology* **22**, 385502. https://doi.org/10.1088/0957-4484/22/38/385502 (2011).

37. Lide, D. R. *CRC Handbook of Chemistry and Physics*. 84th edn, (CRC Press LLC, Boca Raton, 2004).

38. Ghambarian, M., Azizi, Z. & Ghashghaee, M. Hydrogen detection on black phosphorene doped with Ni, Pd, and Pt: Periodic density functional calculations. *Int. J. Hydrog. Energy.* **45**, 16298–16309. https://doi.org/10.1016/j.ijhydene.2020.04.102 (2020).

39. Ghashghaee, M. & Ghambarian, M. Highly improved carbon dioxide sensitivity and selectivity of black phosphorene sensor by vacancy doping: A quantum chemical perspective. *Int. J. Quantum Chem.* **120**, e26265. https://doi.org/10.1002/qua.26265 (2020).

40. Ghashghaee, M., Ghambarian, M. & Azizi, Z. Molecular-level insights into furfural hydrogenation intermediates over single-atomic Cu catalysts on magnesia and silica nanoclusters. *Mol. Simul.* **45**, 154–163. https://doi.org/10.1080/08927022.2018.1547820 (2019).

41. Ghashghaee, M. & Ghambarian, M. Protonation of propene on silica-grafted hydroxylated molybdenum and tungsten oxide metathesis catalysts: A DFT study. *Iran. J. Chem. Chem. Eng.* **38**, 175–187 (2019).

42. Ghashghaee, M., Azizi, Z. & Ghambarian, M. Theoretical insights into hydrogen sensing capabilities of black phosphorene modified through ZnO doping and decoration. *Int. J. Hydrog. Energy.* **45**, 16918–16928. https://doi.org/10.1016/j.ijhydene.2020.04.138 (2020).

43. Ghadiri, M., Ghambarian, M. & Ghashghaee, M. Detection of CNX cyanogen halides (X = F, Cl) on metal-free defective phosphorene sensor: periodic DFT calculations. *Mol. Phys.* https://doi.org/10.1080/00268976.2020.1819577 (2020).

44. Kulish, V. V., Malyi, O. I., Persson, C. & Wu, P. Adsorption of metal adatoms on single-layer phosphorene. *Phys. Chem. Chem. Phys.* **17**, 992–1000. https://doi.org/10.1039/c4cp03890h (2015).

45. Qiao, J., Kong, X., Hu, Z.-X., Yang, F. & Ji, W. High-mobility transport anisotropy and linear dichroism in few-layer black phosphorus. *Nat. Commun.* **5**, 4475. https://doi.org/10.1038/ncomms5475 (2014).

46. Alwarappan, S. & Kumar, A. *Graphene-Based Materials: Science and Technology* (Taylor & Francis Group, Abingdon, 2014).

47. Cui, H. *et al.* Tellurene nanoflake-based NO_2 sensors with superior sensitivity and a sub-parts-per-billion detection limit. *ACS Appl. Mater. Inter.* **12**, 47704–47713. https://doi.org/10.1021/acsami.0c15964 (2020).

48. Xie, Z. *et al.* Two-dimensional borophene: Properties, fabrication, and promising applications. *Research* **2020**, 2624617. https://doi.org/10.34133/2020/2624617 (2020).

49. Morell, C., Gazquez, J. L., Vela, A., Guegan, F. & Chermette, H. Revisiting electroaccepting and electrodonating powers: Proposals for local electrophilicity and local nucleophilicity descriptors. *Phys. Chem. Chem. Phys.* **16**, 26832–26842. https://doi.org/10.1039/c4cp03167a (2014).

50. Ghashghaee, M. & Ghambarian, M. Ethene protonation over silica-grafted metal (Cr, Mo, and W) oxide catalysts: A comparative nanocluster modeling study. *Russ. J. Inorg. Chem.* **63**, 1570–1577. https://doi.org/10.1134/S0036023618160015 (2018).

51. Miranda-Quintana, R. A. & Ayers, P. W. Systematic treatment of spin-reactivity indicators in conceptual density functional theory. *Theor. Chem. Acc.* **135**, 239. https://doi.org/10.1007/s00214-016-1995-5 (2016).

52. Ghambarian, M., Azizi, Z. & Ghashghaee, M. Phosphorene defects for high-quality detection of nitric oxide and carbon monoxide: A periodic density functional study. *Chem. Eng. J.* **396**, 125247. https://doi.org/10.1016/j.cej.2020.125247 (2020).

53. Hu, T. & Hong, J. First-principles study of metal adatom adsorption on black phosphorene. *J. Phys. Chem. C* **119**, 8199–8207. https://doi.org/10.1021/acs.jpcc.5b01300 (2015).

54. Takahashi, T., Tokailin, H., Suzuki, S., Sagawa, T. & Shirotani, I. Electronic band structure of black phosphorus studied by angle-resolved ultraviolet photoelectron spectroscopy. *J. Phys. C Solid State Phys.* **18**, 825–836. https://doi.org/10.1088/0022-3719/18/4/013 (1985).

55. Hutter, J., Iannuzzi, M., Schiffmann, F. & VandeVondele, J. cp2k: Atomistic simulations of condensed matter systems. *WIRES Comput. Mol. Sci.* **4**, 15–25. https://doi.org/10.1002/wcms.1159 (2014).

56. Valiev, M. *et al.* NWChem: A comprehensive and scalable open-source solution for large scale molecular simulations. *Comput. Phys. Commun.* **181**, 1477–1489. https://doi.org/10.1016/j.cpc.2010.04.018 (2010).

57. Lu, T. & Chen, F. Multiwfn: A multifunctional wavefunction analyzer. *J. Comput. Chem.* **33**, 580–592. https://doi.org/10.1002/jcc.22885 (2012).

58. Giannozzi, P. *et al.* QUANTUM ESPRESSO: A modular and open-source software project for quantum simulations of materials. *J. Phys. Condens. Mater.* **21**, 395502. https://doi.org/10.1088/0953-8984/21/39/395502 (2009).

59. Macrae, C. F. *et al.* Mercury CSD 2.0—new features for the visualization and investigation of crystal structures. *J. Appl. Crystallogr.* **41**, 466–470. https://doi.org/10.1107/S0021889807067908 (2008).

60. Hanwell, M. D. *et al.* Avogadro: An advanced semantic chemical editor, visualization, and analysis platform. *J. Cheminform.* https://doi.org/10.1186/1758-2946-1184-1117 (2012).

Acknowledgements

Author contributions

A.M. contributed to formal analysis, writing—original draft, writing—review & editing, and resources. M.G. (the second author) contributed to conceptualization, data curation, methodology, software, formal analysis, and resources. M.G. (the third author) contributed to conceptualization, formal analysis, project administration, validation, visualization, writing—original draft, and writing—review & editing.

Competing interests

The authors declare no competing interests.

Additional information

Supplementary Information The online version contains supplementary material available at https://doi.org/10.1038/s41598-020-80343-9.

Correspondence and requests for materials should be addressed to M.G.

Reprints and permissions information is available at www.nature.com/reprints.

Publisher's note Springer Nature remains neutral with regard to jurisdictional claims in published maps and institutional affiliations.